NUWC-NPT Technical Report 11,412
10 February 2003

A Method for Estimating the Mechanical Properties of a Solid Material Subjected to Significant Compressional Forces — Part I: Numerical Theoretical Solution for a Single Thick Plate

Andrew J. Hull
Submarine Sonar Department

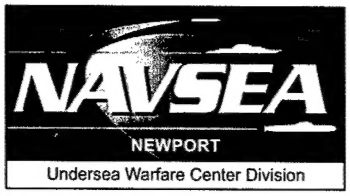

Naval Undersea Warfare Center Division
Newport, Rhode Island

PREFACE

This report was prepared under NUWC Division Newport Job Order No. 701Y070.

The technical reviewer for this report was Donald L. Cox (Code 2133).

The author wishes to thank Karen Holt (Code 5431) for her help with the editing of the manuscript.

Reviewed and Approved: 10 February 2003

Frank W. Molino
Head (Acting), Submarine Sonar Department

REPORT DOCUMENTATION PAGE

Form Approved
OMB No. 0704-0188

1. AGENCY USE ONLY *(Leave blank)*	2. REPORT DATE	3. REPORT TYPE AND DATES COVERED
	10 February 2003	

4. TITLE AND SUBTITLE

A Method for Estimating the Mechanical Properties of a Solid Material Subjected to Significant Compressional Forces — Part I: Numerical Theoretical Solution for a Single Thick Plate

5. FUNDING NUMBERS

6. AUTHOR(S)

Andrew J. Hull

7. PERFORMING ORGANIZATION NAME(S) AND ADDRESS(ES)

Naval Undersea Warfare Center Division
1176 Howell Street
Newport, RI 02841-1708

8. PERFORMING ORGANIZATION REPORT NUMBER

TR 11,412

9. SPONSORING/MONITORING AGENCY NAME(S) AND ADDRESS(ES)

10. SPONSORING/MONITORING AGENCY REPORT NUMBER

11. SUPPLEMENTARY NOTES

12a. DISTRIBUTION/AVAILABILITY STATEMENT

Approved for public release; distribution is unlimited.

12b. DISTRIBUTION CODE

13. ABSTRACT (Maximum 200 words)

This report develops a technique for measuring (or estimating) the complex frequency-dependent dilatational and shear wavenumbers of a single slab of material subjected to large static compressional forces. The method employs two transfer functions that are obtained by vibrating the mass-loaded material in both the vertical and horizontal directions. Once this process is accomplished, the transfer functions are merged with a theoretical model and displayed as analytical surfaces from which the dilatational and shear wavenumbers can be identified and estimated. These wavenumbers are then combined to determine complex dilatational wavespeed, complex shear wavespeed, complex Lamé constants, complex Young's modulus, complex shear modulus, and complex Poisson's ratio.

14. SUBJECT TERMS

Dilatational Wavespeed Estimates
Mechanical Property Estimates
Shear Wavespeed Measurements
Solid Material Measurements
Thick Plate Theory

15. NUMBER OF PAGES
52

16. PRICE CODE

17. SECURITY CLASSIFICATION OF REPORT	18. SECURITY CLASSIFICATION OF THIS PAGE	19. SECURITY CLASSIFICATION OF ABSTRACT	20. LIMITATION OF ABSTRACT
Unclassified	Unclassified	Unclassified	SAR

TABLE OF CONTENTS

LIST OF ILLUSTRATIONS

LIST OF ILLUSTRATIONS (Cont'd)

LIST OF TABLES

A METHOD FOR ESTIMATING THE MECHANICAL PROPERTIES OF A SOLID MATERIAL SUBJECTED TO SIGNIFICANT COMPRESSIONAL FORCES — PART I: NUMERICAL THEORETICAL SOLUTION FOR A SINGLE THICK PLATE

1. INTRODUCTION

The mechanical properties of materials create displacement and stress fields that often contribute significantly to the static and dynamic response of the structures in which they are found. One important characteristic shared by most elastomeric materials (especially slab-shaped plates) is the change that occurs in their mechanical properties when the elastomer is subjected to large compressional or tensile forces. Under these forces, the rigidity of the material typically becomes larger and the damping factors become smaller. A thorough understanding of such behavior is necessary so that the static and dynamic responses of a material can be correctly included in mathematical models, as well as properly understood in the actual physical structure itself.

Some of the numerous methods developed to determine the properties of various materials, include those based on the use of resonance[1-4] and transfer function data.[3,5-7] Several parameter estimation techniques have also been investigated for plates.[8-11] Although the above approaches do not allow for testing under significant compressional forces, efforts have been made to measure material properties under large pressures.[12-14] In such research, the material is placed in a pressurized setting and insonified, after which its response is measured. However, these procedures, which are typically conducted under extreme atmospheric pressure in the laboratory, can have an adverse effect on instrumentation, as well as on safety. In other studies,[15,16] a mass-loaded, long, thin rod has been examined with respect to the bar wavespeed and corresponding Young's modulus (shear motion is not addressed).

This report describes an inverse method that has been developed to measure complex, frequency-dependent dilatational and shear wavenumbers of a single slab-shaped material subjected to large compressional forces. Based on thick plate theory, the linear equations of motion of the system are first derived for a test specimen that is attached to a shaker at the

bottom and a mass at the top. A typical test configuration is shown in figures 1 and 2, where the shaker projects mechanical energy onto a plate-shaped material that is mass loaded. Two transfer function measurements are obtained by vibrating the mass-loaded material in both the vertical and horizontal directions. Once this process is accomplished, the transfer functions are combined to yield closed-form values of the dilatational and shear wavenumbers at any given test frequency. After these parameters are estimated, calculations can be made for the complex, frequency-dependent dilatational and shear wavespeeds; Young's and shear moduli; and Poisson's ratio.

The above method is intended for use with materials that are to be placed in an environment where they will be subjected to large compressional forces, such as those that would typically arise in submarines, where the panels that coat the exterior of the ship are exposed to a wide range of hydrostatic pressures.

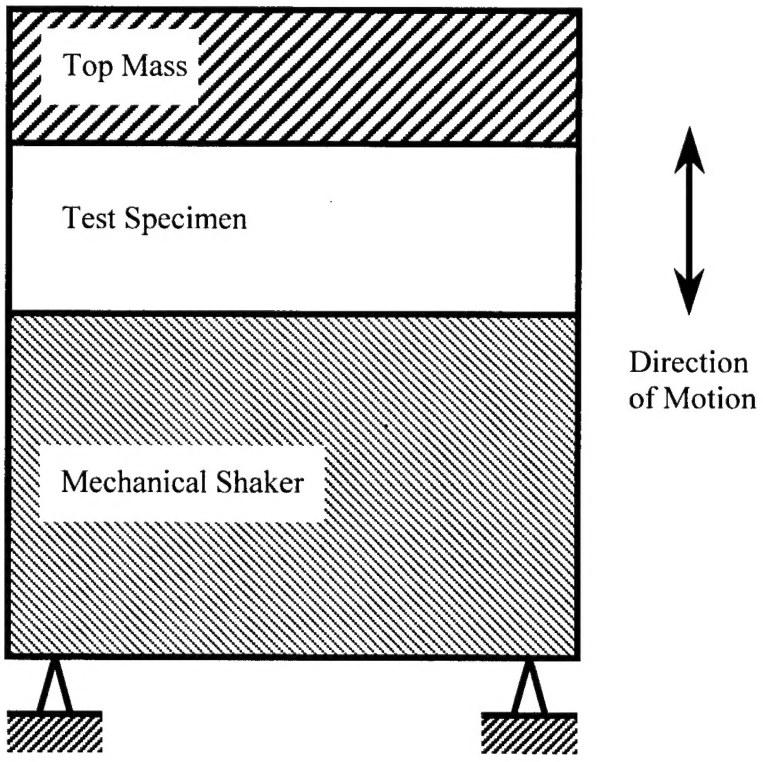

Figure 1. Vertical Motion Test

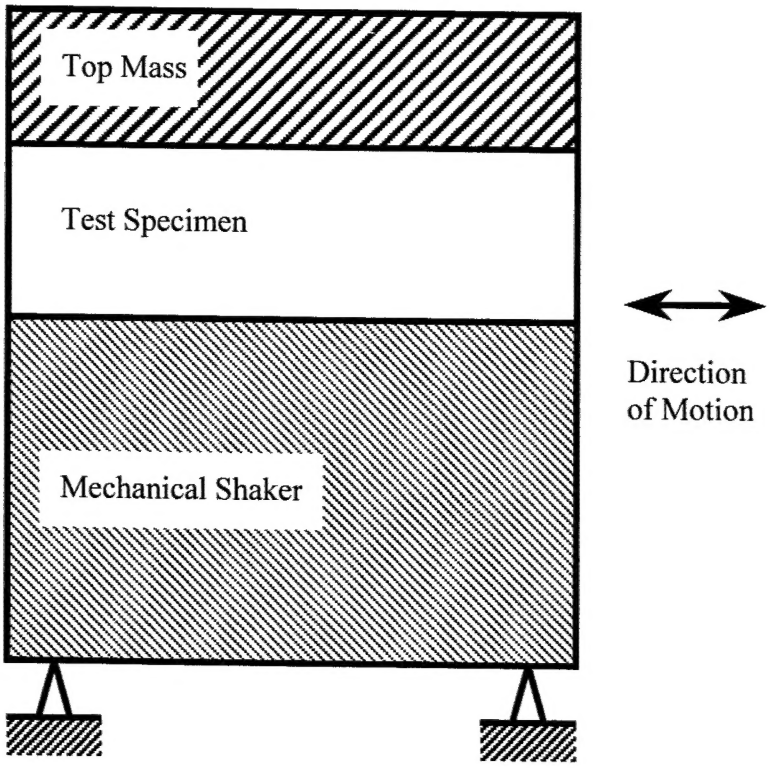

Figure 2. Horizontal Motion Test

2. SYSTEM MODEL

The motion of the test specimen shown in figures 1 and 2 is governed by the equation

$$\mu\nabla^2\mathbf{u} + (\lambda + \mu)\nabla\nabla \bullet \mathbf{u} = \rho\frac{\partial^2\mathbf{u}}{\partial t^2}\,, \tag{1}$$

where λ and μ are the complex Lamé constants (N/m^2), ρ is the density (kg/m^3), t is time (s), $\bullet$ denotes a vector dot product, and $\mathbf{u}$ is the Cartesian coordinate displacement vector of the material. The coordinate system of the test configuration is shown in figure 3. Note that using this orientation results in $b = 0$ and a having a value less than zero. The thickness

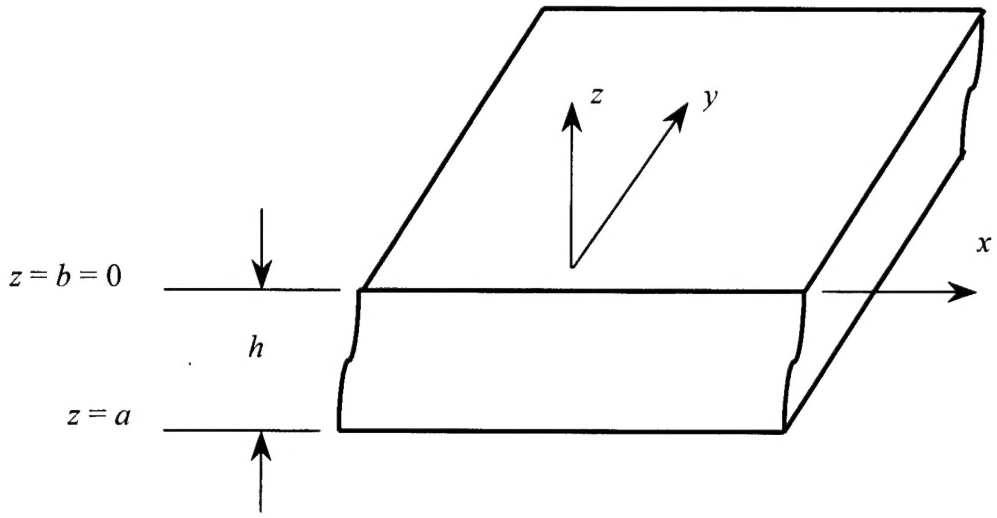

Figure 3. Coordinate System of Test Specimen Used in Model

of specimen h is a positive value. Equation (1) is manipulated by writing the displacement vector **u** as

$$\mathbf{u} = \begin{Bmatrix} u_x(x,y,z,t) \\ u_y(x,y,z,t) \\ u_z(x,y,z,t) \end{Bmatrix}, \tag{2}$$

where x is the location along the plate (m), y is the location into the plate (m), and z is the location normal to the plate (m), as shown in the figure. The symbol ∇ in equation (1) is the gradient vector differential operator written in three-dimensional Cartesian coordinates as

$$\nabla = \frac{\partial}{\partial x} i_x + \frac{\partial}{\partial y} i_y + \frac{\partial}{\partial z} i_z , \tag{3}$$

with i_x denoting the unit vector in the x-direction, i_y denoting the unit vector in the y-direction, and i_z denoting the unit vector in the z-direction; ∇^2 is the three-dimensional Laplace operator operating on vector **u** as

$$\nabla^2 \mathbf{u} = \nabla^2 u_x i_x + \nabla^2 u_y i_y + \nabla^2 u_z i_z \tag{4}$$

and operating on scalar u as

$$\nabla^2 u_{x,y,z} = \nabla \bullet \nabla u_{x,y,z} = \frac{\partial^2 u_{x,y,z}}{\partial x^2} + \frac{\partial^2 u_{x,y,z}}{\partial y^2} + \frac{\partial^2 u_{x,y,z}}{\partial z^2} \ . \tag{5}$$

The term $\nabla \bullet \mathbf{u}$ is called the divergence and is equal to

$$\nabla \bullet \mathbf{u} = \frac{\partial u_x}{\partial x} + \frac{\partial u_y}{\partial y} + \frac{\partial u_z}{\partial z} \ . \tag{6}$$

The displacement vector $\mathbf{u}$ is written as

$$\mathbf{u} = \nabla \phi + \nabla \times \vec{\psi} \ , \tag{7}$$

where ϕ is a dilatational scalar potential, $\times$ denotes a vector crossproduct, and $\vec{\psi}$ is an equi-voluminal vector potential expressed as

$$\vec{\psi} = \begin{Bmatrix} \psi_x(x,y,z,t) \\ \psi_y(x,y,z,t) \\ \psi_z(x,y,z,t) \end{Bmatrix} . \tag{8}$$

The problem is formulated as a two-dimensional system; thus $y \equiv 0$, $u_y(x,y,z,t) \equiv 0$, and $\partial(\cdot)/\partial y \equiv 0$. Expanding equation (7) and breaking the displacement vector into its individual nonzero terms yields

$$u_x(x,z,t) = \frac{\partial \phi(x,z,t)}{\partial x} - \frac{\partial \psi_y(x,z,t)}{\partial z} \tag{9}$$

and

$$u_z(x,z,t) = \frac{\partial \phi(x,z,t)}{\partial z} + \frac{\partial \psi_y(x,z,t)}{\partial x} \ . \tag{10}$$

Equations (9) and (10) are next inserted into equation (1), which results in

$$c_d^2 \nabla^2 \phi(x,z,t) = \frac{\partial^2 \phi(x,z,t)}{\partial t^2} \tag{11}$$

and

$$c_s^2 \nabla^2 \psi_y(x,z,t) = \frac{\partial^2 \psi_y(x,z,t)}{\partial t^2}, \tag{12}$$

where equation (11) corresponds to the dilatational component and equation (12) corresponds to the shear component of the displacement field. Correspondingly, the constants c_d and c_s are the complex dilatational and shear wavespeeds, respectively, and are determined by

$$c_d = \sqrt{\frac{\lambda + 2\mu}{\rho}} \tag{13}$$

and

$$c_s = \sqrt{\frac{\mu}{\rho}}. \tag{14}$$

The relationship of the Lamé constants to the Young's and shear moduli is shown as

$$\lambda = \frac{E\upsilon}{(1+\upsilon)(1-2\upsilon)} \tag{15}$$

and

$$\mu = G = \frac{E}{2(1+\upsilon)}, \tag{16}$$

where E is the complex Young's modulus ($\mathrm{N/m^2}$), G is the complex shear modulus ($\mathrm{N/m^2}$), and υ is the Poisson's ratio of the material (dimensionless).

The conditions of infinite length and steady-state response are now imposed, allowing the scalar and vector potential to be written as

$$\phi(x,z,t) = \Phi(z)\exp(\mathrm{i}kx)\exp(\mathrm{i}\omega t) \tag{17}$$

and

$$\psi_y(x,z,t) = \Psi(z)\exp(\mathrm{i}kx)\exp(\mathrm{i}\omega t) \ , \tag{18}$$

where i is the square root of –1, ω is frequency (rad/s), and k is wavenumber with respect to the x-axis (rad/m). Inserting equation (17) into equation (11) yields

$$\frac{d^2\Phi(z)}{dz^2} + \alpha^2\Phi(z) = 0 \ , \tag{19}$$

where

$$\alpha = \sqrt{k_d^2 - k^2} \ , \tag{20}$$

with

$$k_d = \frac{\omega}{c_d} \ . \tag{21}$$

Inserting equation (18) into equation (12) yields

$$\frac{d^2\Psi(z)}{dz^2} + \beta^2\Psi(z) = 0 \ , \tag{22}$$

where

$$\beta = \sqrt{k_s^2 - k^2} \ , \tag{23}$$

with

$$k_s = \frac{\omega}{c_s} \ . \tag{24}$$

The solution to equation (19) is

$$\Phi(z) = A(k,\omega)\exp(\mathrm{i}\alpha z) + B(k,\omega)\exp(-\mathrm{i}\alpha z) \ , \tag{25}$$

and the solution to equation (22) is

$$\Psi(z) = C(k,\omega)\exp(\mathrm{i}\beta z) + D(k,\omega)\exp(-\mathrm{i}\beta z) \ , \tag{26}$$

where $A(k,\omega)$, $B(k,\omega)$, $C(k,\omega)$, and $D(k,\omega)$ are wave response coefficients that are determined later in section 3. The displacements, now written as functions of the unknown constants using the expressions in equations (9) and (10), are

$$\begin{aligned} u_z(x,z,t) &= U_z(k,z,\omega)\exp(\mathrm{i}kx)\exp(\mathrm{i}\omega t) \\ &= \{\mathrm{i}\alpha[A(k,\omega)\exp(\mathrm{i}\alpha z) - B(k,\omega)\exp(-\mathrm{i}\alpha z)] \\ &\quad + \mathrm{i}k[C(k,\omega)\exp(\mathrm{i}\beta z) + D(k,\omega)\exp(-\mathrm{i}\beta z)]\}\exp(\mathrm{i}kx)\exp(\mathrm{i}\omega t) \end{aligned} \tag{27}$$

and

$$\begin{aligned} u_x(x,z,t) &= U_x(k,z,\omega)\exp(\mathrm{i}kx)\exp(\mathrm{i}\omega t) \\ &= \{\mathrm{i}k[A(k,\omega)\exp(\mathrm{i}\alpha z) + B(k,\omega)\exp(-\mathrm{i}\alpha z)] \\ &\quad -. \mathrm{i}\beta[C(k,\omega)\exp(\mathrm{i}\beta z) - D(k,\omega)\exp(-\mathrm{i}\beta z)]\}\exp(\mathrm{i}kx)\exp(\mathrm{i}\omega t) \ . \end{aligned} \tag{28}$$

In the next step, specific boundary conditions must be provided to obtain the individual solutions for vertical motion (section 3) and horizontal motion (section 4).

3. TRANSFER FUNCTION FOR VERTICAL MOTION

For the case of vertical motion, the base at $z = a$ is vibrated vertically with a shaker (see figure 1). Formulating this problem requires definition of the four boundary conditions, as shown next.

Because a rigid mass is attached to the material and the particle motion is vertical, the tangential (horizontal) motion at the top of the plate ($z = b$) is zero, with this equation written as

$$u_x(x,b,t) = 0 \ . \tag{29}$$

The normal stress at the top of the specimen is equal to the opposite of the load created by the mass in the z-direction. This expression is

$$\tau_{zz}(x,b,t) = (\lambda + 2\mu)\frac{\partial u_z(x,b,t)}{\partial z} + \lambda \frac{\partial u_x(x,b,t)}{\partial x} = -M \frac{\partial^2 u_z(x,b,t)}{\partial t^2} \ , \tag{30}$$

where M is mass per unit area ($\mathrm{kg/m^2}$) of the attached mass. The tangential motion at the bottom of the plate ($z = a$) is zero and is shown as

$$u_x(x,a,t) = 0 \ . \tag{31}$$

The normal motion at the bottom of the plate (prescribed as a system input) is written as

$$u_z(x,a,t) = U_0 \exp(\mathrm{i}\omega t) \ . \tag{32}$$

Assembling equations (1)–(32) and letting $b = 0$ yields the four-by-four set of linear equations that model the system as

$$\mathbf{Ax} = \mathbf{b} \ , \tag{33}$$

where the entries of equation (33) are

$$A_{11} = \mathrm{i}k \ , \tag{34}$$

$$A_{12} = A_{11} \ , \tag{35}$$

$$A_{13} = -\mathrm{i}\beta \ , \tag{36}$$

$$A_{14} = -A_{13} \ , \tag{37}$$

$$A_{21} = -\alpha^2\lambda - 2\alpha^2\mu - \lambda k^2 - \mathrm{i}M\omega^2\alpha \ , \tag{38}$$

$$A_{22} = -\alpha^2\lambda - 2\alpha^2\mu - \lambda k^2 + \mathrm{i}M\omega^2\alpha \ , \tag{39}$$

$$A_{23} = -2k\beta\mu - \mathrm{i}M\omega^2 k \ , \tag{40}$$

$$A_{24} = 2k\beta\mu - \mathrm{i}M\omega^2 k \ , \tag{41}$$

$$A_{31} = A_{11}\exp(\mathrm{i}\alpha a) \ , \tag{42}$$

$$A_{32} = A_{11}\exp(-\mathrm{i}\alpha a) \ , \tag{43}$$

$$A_{33} = A_{13}\exp(\mathrm{i}\beta a) \ , \tag{44}$$

$$A_{34} = -A_{13}\exp(-\mathrm{i}\beta a) \ , \tag{45}$$

$$A_{41} = \mathrm{i}\alpha\exp(\mathrm{i}\alpha a) \ , \tag{46}$$

$$A_{42} = -\mathrm{i}\alpha\exp(-\mathrm{i}\alpha a) \ , \tag{47}$$

$$A_{43} = \mathrm{i}k\exp(\mathrm{i}\beta a) \ , \tag{48}$$

$$A_{44} = \mathrm{i}k\exp(-\mathrm{i}\beta a) \ , \tag{49}$$

$$x_{11} = A(k,\omega) \ , \tag{50}$$

$$x_{21} = B(k,\omega) \ , \tag{51}$$

$$x_{31} = C(k,\omega) \ , \tag{52}$$

$$x_{41} = D(k,\omega) \ , \tag{53}$$

$$b_{11} = 0 \ , \tag{54}$$

$$b_{21} = 0 \ , \tag{55}$$

$$b_{31} = 0 \ , \tag{56}$$

and

$$b_{41} = U_0 \ . \tag{57}$$

From equations (34)-(57), the solution to the constants $A(k,\omega)$, $B(k,\omega)$, $C(k,\omega)$, and $D(k,\omega)$ can be calculated at each specific wavenumber and frequency from

$$\mathbf{x} = \mathbf{A}^{-1}\mathbf{b} \ . \tag{58}$$

Noting that $k = 0$ for vertical motion and using the coefficients from equation (58) results in the transfer function between the vertical base displacement and the vertical mass displacement being written as

$$T_1(\omega) = \frac{1}{R_1(\omega)} = \frac{U_z(0,b,\omega)}{U_0} = \frac{1}{\cos(k_d h) - \left(\frac{M}{\rho}\right) k_d \sin(k_d h)} , \tag{59}$$

where $T_1(\omega)$ or $R_1(\omega)$ corresponds to the frequency-domain data from the vertical motion experiment, which are typically obtained by applying a Fourier transform to raw time-domain data collected with accelerometers or laser velocimeters.

4. TRANSFER FUNCTION FOR HORIZONTAL MOTION

For the case of horizontal motion, the base at $z = a$ is vibrated horizontally with a shaker (see figure 2). Formulating this problem requires definition of the four boundary conditions, as shown next.

Because a rigid mass is attached to the material and the particle motion is horizontal, the shear (tangential) stress at the top of the plate is equal to the opposite of the load created by the mass in the x-direction. This expression is

$$\tau_{zx}(x,b,t) = \mu\left[\frac{\partial u_x(x,b,t)}{\partial z} + \frac{\partial u_z(x,b,t)}{\partial x}\right] = -M\frac{\partial^2 u_x(x,b,t)}{\partial t^2} , \tag{60}$$

where M is the mass per unit area ($\mathrm{kg/m^2}$) of the attached mass. The normal motion at the top of the plate ($z = b$) is zero, with this equation written as

$$u_z(x,b,t) = 0 . \tag{61}$$

The tangential motion at the bottom of the plate ($z = a$), prescribed as a system input, is shown as

$$u_x(x,a,t) = V_0 \exp(\mathrm{i}\omega t) , \tag{62}$$

and the normal motion at the bottom of the plate is zero, which is expressed as

$$u_z(x,a,t) = 0 \ . \tag{63}$$

Assembling equations (1)–(28) and (60)–(63) and letting $b = 0$ yields the four-by-four set of linear equations that model the system as

$$\mathbf{Ax} = \mathbf{b} \ , \tag{64}$$

where the entries of equation (64) are

$$A_{11} = -2\mu k\alpha - \mathrm{i}\omega^2 Mk \ , \tag{65}$$

$$A_{12} = 2\mu k\alpha - \mathrm{i}\omega^2 Mk \ , \tag{66}$$

$$A_{13} = \mu\beta^2 - \mu k^2 + \mathrm{i}\omega^2 M\beta \ , \tag{67}$$

$$A_{14} = \mu\beta^2 - \mu k^2 - \mathrm{i}\omega^2 M\beta \ , \tag{68}$$

$$A_{21} = \mathrm{i}\alpha \ , \tag{69}$$

$$A_{22} = -A_{21} \ , \tag{70}$$

$$A_{23} = \mathrm{i}k \ , \tag{71}$$

$$A_{24} = A_{23} \ , \tag{72}$$

$$A_{31} = A_{23}\exp(\mathrm{i}\alpha a) \ , \tag{73}$$

$$A_{32} = A_{23}\exp(-\mathrm{i}\alpha a) \ , \tag{74}$$

$$A_{33} = -\mathrm{i}\beta\exp(\mathrm{i}\beta a) \ , \tag{75}$$

$$A_{34} = \mathrm{i}\beta\exp(-\mathrm{i}\beta a) \ , \tag{76}$$

$$A_{41} = A_{21}\exp(\mathrm{i}\alpha a) \ , \tag{77}$$

$$A_{42} = -A_{21}\exp(-\mathrm{i}\alpha a) \ , \tag{78}$$

$$A_{43} = A_{23}\exp(\mathrm{i}\beta a) \ , \tag{79}$$

$$A_{44} = A_{23}\exp(-\mathrm{i}\beta a) \ , \tag{80}$$

$$x_{11} = A(k,\omega) \ , \tag{81}$$

$$x_{21} = B(k,\omega) \ , \tag{82}$$

$$x_{31} = C(k,\omega) \ , \tag{83}$$

$$x_{41} = D(k,\omega) \ , \tag{84}$$

$$b_{11} = 0 \ , \tag{85}$$

$$b_{21} = 0 \ , \tag{86}$$

$$b_{31} = V_0 \ , \tag{87}$$

and

$$b_{41} = 0 \ . \tag{88}$$

Equations (65)-(88) allow calculation of the solution to the constants $A(k,\omega)$, $B(k,\omega)$, $C(k,\omega)$,and $D(k,\omega)$ at each specific wavenumber and frequency from

$$\mathbf{x} = \mathbf{A}^{-1}\mathbf{b} \ . \tag{89}$$

Noting that $k = 0$ for horizontal motion and using the coefficients from equation (89) results in the transfer function between the horizontal base displacement and the horizontal mass displacement being written as

$$T_2(\omega) = \frac{1}{R_2(\omega)} = \frac{U_x(0,b,\omega)}{V_0} = \frac{1}{\cos(k_s h) - \left(\frac{M}{\rho}\right) k_s \sin(k_s h)} \ , \tag{90}$$

where $T_2(\omega)$ or $R_2(\omega)$ corresponds to the frequency-domain data from the horizontal motion experiment.

5. INVERSE SOLUTION FOR SYSTEM WITHOUT MASS

Although designed for the testing of materials subjected to compressional forces, the experiment can also be conducted without these forces, as described next. This simpler version without the mass has an inverse solution that is a closed-form expression — which does not occur when the mass is added to the experiment and corresponding analysis. When mass is not present in the experiment, equations (59) and (90) become

$$T_3(\omega) = \frac{1}{R_3(\omega)} = \frac{U_z(0,b,\omega)}{U_0} = \frac{1}{\cos(k_d h)} \tag{91}$$

and

$$T_4(\omega) = \frac{1}{R_4(\omega)} = \frac{U_x(0,b,\omega)}{V_0} = \frac{1}{\cos(k_s h)}\ , \tag{92}$$

respectively. Inverting equation (91) yields the value of k_d as a function of R_3. The solution for the real part of k_d is

$$\mathrm{Re}(k_d) = \begin{cases} \dfrac{1}{2h}\mathrm{Arccos}(s) + \dfrac{n\pi}{2h} & n \text{ even} \\ \dfrac{1}{2h}\mathrm{Arccos}(-s) + \dfrac{n\pi}{2h} & n \text{ odd} \end{cases}\ , \tag{93}$$

where

$$s = [\mathrm{Re}(R_3)]^2 + [\mathrm{Im}(R_3)]^2 - \sqrt{\left\{[\mathrm{Re}(R_3)]^2 + [\mathrm{Im}(R_3)]^2\right\}^2 - \left\{2[\mathrm{Re}(R_3)]^2 - 2[\mathrm{Im}(R_3)]^2 - 1\right\}}\ , \tag{94}$$

n is a non-negative integer, and capital A denotes the principal value of the inverse cosine function. The value of n is determined from the function s, which is a cosine function with respect to frequency. At zero frequency, n is 0. Every time s cycles through π radians (180°), n is increased by 1. After the solution to the real part of k_d is found, the solution to the imaginary part is written as

$$\mathrm{Im}(k_d) = \frac{1}{h}\log_e\left\{\frac{\mathrm{Re}(R_3)}{\cos[\mathrm{Re}(k_d)h]} - \frac{\mathrm{Im}(R_3)}{\sin[\mathrm{Re}(k_d)h]}\right\}\ . \tag{95}$$

The inverse solution to equation (92) is the same as that for equation (91) and is written as

$$\mathrm{Re}(k_s) = \begin{cases} \dfrac{1}{2h}\mathrm{Arccos}(r) + \dfrac{m\pi}{2h} & m \text{ even} \\ \dfrac{1}{2h}\mathrm{Arccos}(-r) + \dfrac{m\pi}{2h} & m \text{ odd} \end{cases}\ , \tag{96}$$

where

$$r = [\mathrm{Re}(R_4)]^2 + [\mathrm{Im}(R_4)]^2 - \sqrt{\left\{[\mathrm{Re}(R_4)]^2 + [\mathrm{Im}(R_4)]^2\right\}^2 - \left\{2[\mathrm{Re}(R_4)]^2 - 2[\mathrm{Im}(R_4)]^2 - 1\right\}}\,, \tag{97}$$

m is a non-negative integer, and capital A denotes the principal value of the inverse cosine function. The value of m is determined from the function r, which is a cosine function with respect to frequency. At zero frequency, m is 0. Every time r cycles through π radians (180°), m is increased by 1. After the solution to the real part of k_s is found, the solution to the imaginary part is written as

$$\mathrm{Im}(k_s) = \frac{1}{h}\log_e\left\{\frac{\mathrm{Re}(R_4)}{\cos[\mathrm{Re}(k_s)h]} - \frac{\mathrm{Im}(R_4)}{\sin[\mathrm{Re}(k_s)h]}\right\}. \tag{98}$$

6. INVERSE SOLUTION FOR SYSTEM WITH MASS

Next solved is the inverse problem for vertical and horizontal motion with a mass attached to the plate. This procedure involves use of the experimental data and equations (59) and (90) to estimate the dilatational and shear wavenumbers, respectively. Equations (59) and (90) can be rewritten as

$$f(k_d) = 0 = \cos(k_d h) - \left(\frac{M}{\rho}\right) k_d \sin(k_d h) - R_1 \tag{99}$$

and

$$f(k_s) = 0 = \cos(k_s h) - \left(\frac{M}{\rho}\right) k_s \sin(k_s h) - R_2\,, \tag{100}$$

respectively, where the problem now becomes finding the zeros of the right-hand side of equations (99) and (100) or, in the presence of actual data that contain noise, finding the relative

minima of the right-hand side of equations (99) and (100) and then determining which relative minimum corresponds to dilatational and shear wave propagation and which relative minima are extraneous. Because equations (99) and (100) have a number of relative minima, zero-finding algorithms are not applied to this function, as they typically do not find all the minima locations and are highly dependent on initial starting locations. The best method for finding all minima locations is to plot the absolute value of the right-hand side of equations (99) and (100) as surfaces, with the real part of the wavenumber (k_d or k_s) on one axis and the imaginary part of the wavenumber (k_d or k_s) on the other. At the lower frequencies, the minimum farthest to the left will correspond to dilatational or shear wave propagation. As the frequency increases, extraneous minima will appear to the left of the minimum that corresponds to dilatational or shear wave propagation; however, the wave propagation minimum will always be close to the previous test frequency wave propagation minimum provided that the frequency increments are relatively small.

Also, because the real part of the both the dilatational and shear wavenumbers are monotonically increasing functions with respect to frequency, each increase in frequency will require that the real part of the new wavenumber that is estimated be greater than the real part of the old wavenumber that was previously estimated. Sometimes referred to as a grid method, this process is illustrated in section 8.

7. DETERMINATION OF PROPERTIES FROM WAVENUMBERS

The material properties can be calculated from the wavenumbers. First, the dilatational and shear wavespeeds are determined from

$$c_d = \frac{\omega}{k_d} \tag{101}$$

and

$$c_s = \frac{\omega}{k_s} , \tag{102}$$

respectively. Next, the Lamé constants are calculated from equations (13) and (14), now written as

$$\mu = \rho c_s^2 \tag{103}$$

and

$$\lambda = \rho c_d^2 - 2\rho c_s^2 . \tag{104}$$

Poisson's ratio is then determined from

$$\upsilon = \frac{\lambda}{2(\mu + \lambda)} , \tag{105}$$

Young's modulus from

$$E = \frac{2\mu(2\mu + 3\lambda)}{2(\mu + \lambda)} , \tag{106}$$

and the shear modulus directly from

$$G \equiv \mu . \tag{107}$$

8. NUMERICAL SIMULATION

The above measurement method can be simulated by means of a numerical example, with the values for the soft rubberlike material properties of the test specimen expressed as follows: uncompressed Young's modulus E of $[(1e8 - i2e7) + (5e3f - i3e2f)]$ in N/m^2 (where f is frequency in Hertz), Poisson's ratio υ of 0.40 (dimensionless), density ρ of 1200 kg/m^3, and thickness h of 0.1 m. The top mass is a 0.0254-m (1-inch) steel plate that has a mass per unit area value M of 199 kg/m^2. With this mass value, the compressed Young's modulus of the test specimen is 1.5 times the uncompressed value. The system is first analyzed without the mass, using the closed-form solution method developed in section 5. Next, the mass is added to the plate and the grid method developed in section 6 is applied to the simulated data.

The simulations are conducted with three different amounts of additive noise: no additive noise, 2% additive noise, and 4% additive noise. Additive noise is included in the transfer function with the equation

$$T_e(\omega) = T(\omega) + e\{\mathrm{Re}[T(\omega)]\sigma_a + \mathrm{iIm}[T(\omega)]\sigma_b\} \ , \tag{108}$$

where e is the amount of additive noise added to the transfer function and σ_a and σ_b are random numbers with zero mean and a variance of one. The value e is also called the transfer function error value, and it represents the deviation of the transfer function from perfect data.

Figure 4 plots the transfer function of the system for vertical motion without the mass and corresponds to equation (59) with $M = 0$. Figure 5 illustrates the transfer function of the system for horizontal motion without the mass and corresponds to equation (90) with $M = 0$. In both figures, the top plot is the magnitude in decibels and the bottom plot is the phase angle in degrees.

Figure 6 is a plot of the function s versus frequency and corresponds to equation (94). Figure 7 is a plot of the function r versus frequency and corresponds to equation (97).

All the plots in figures 4 through 7 are displayed without additive noise.

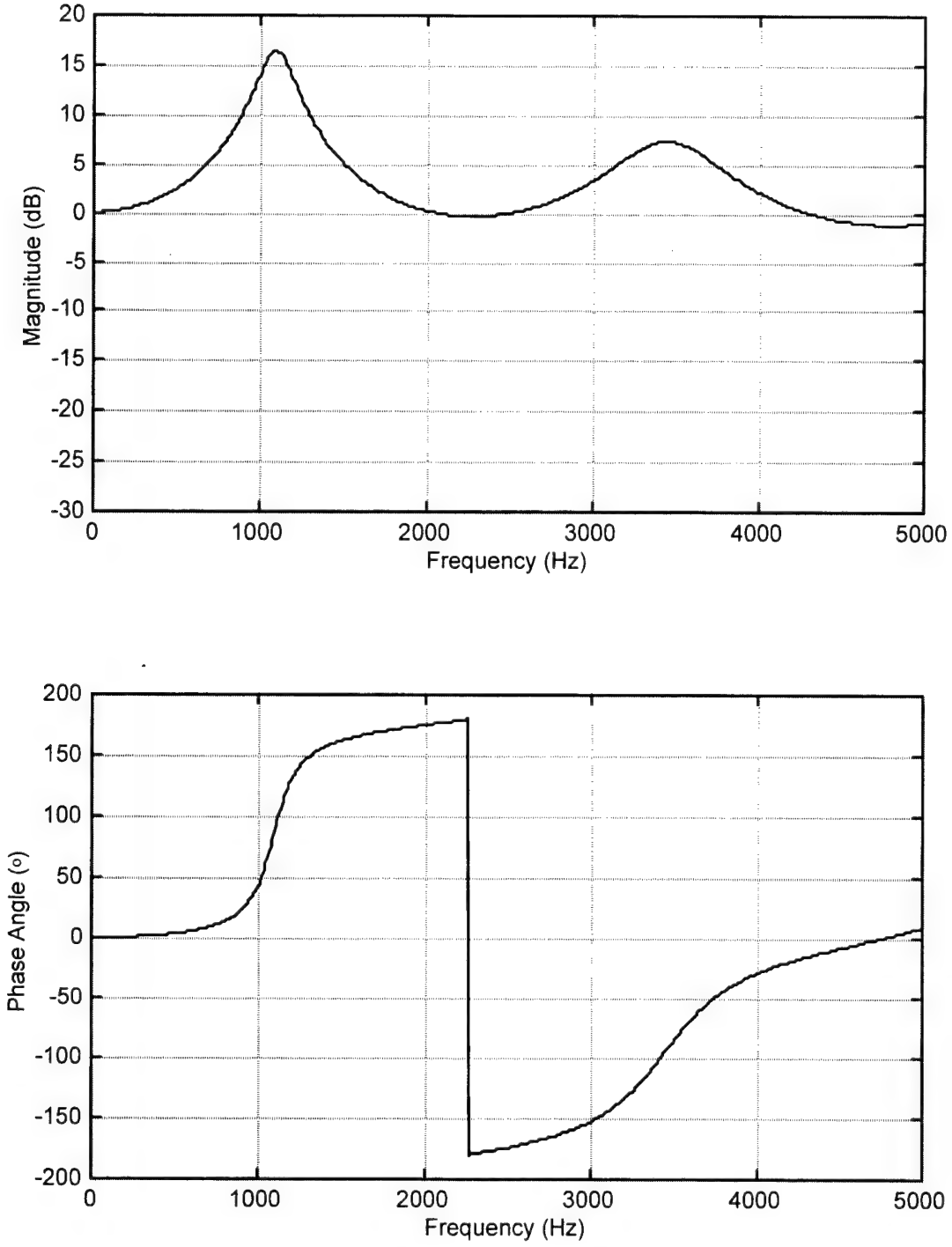

Figure 4. Transfer Function of Vertical Motion Versus Frequency for System Without Mass

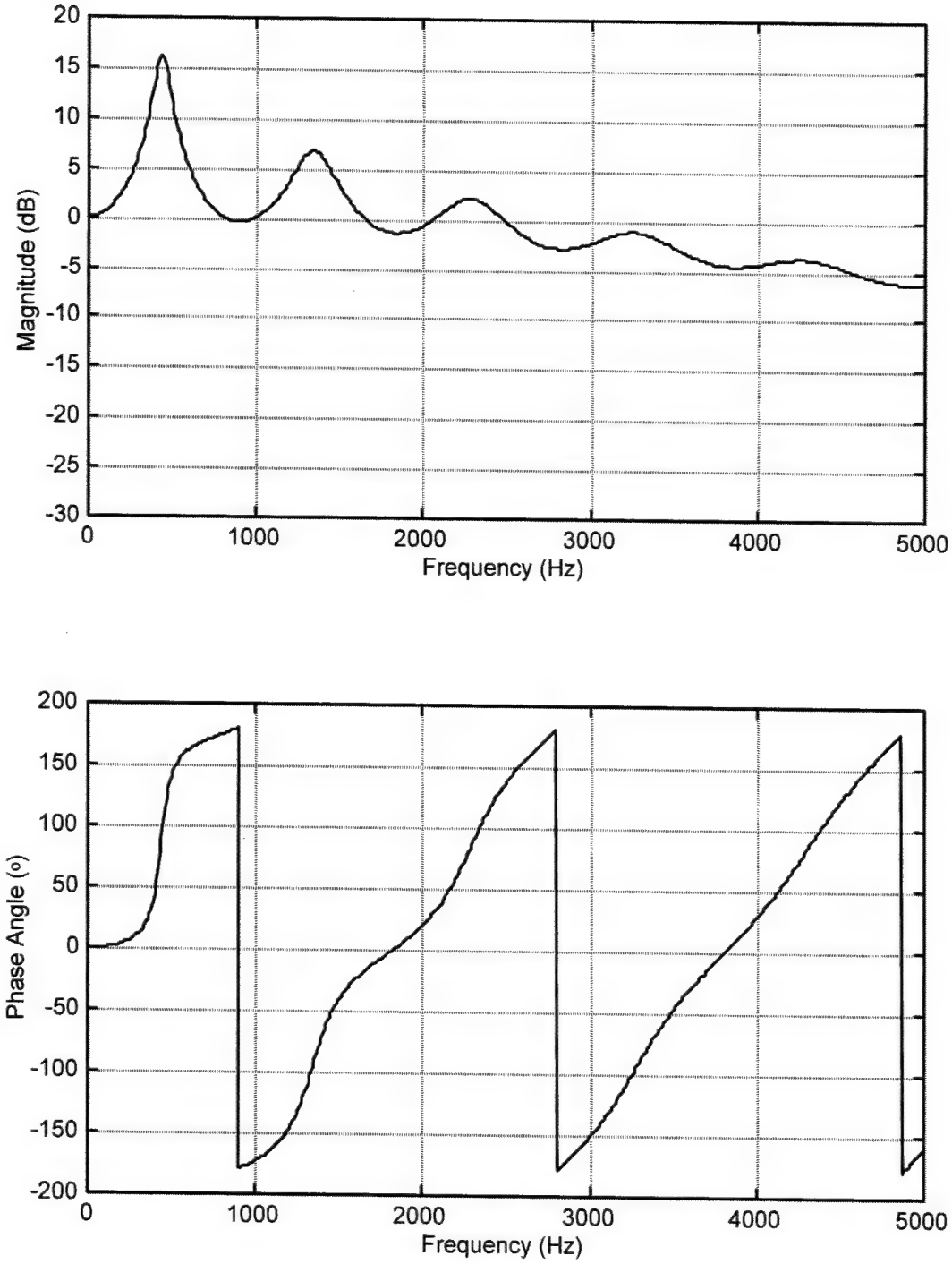

Figure 5. Transfer Function of Horizontal Motion Versus Frequency for System Without Mass

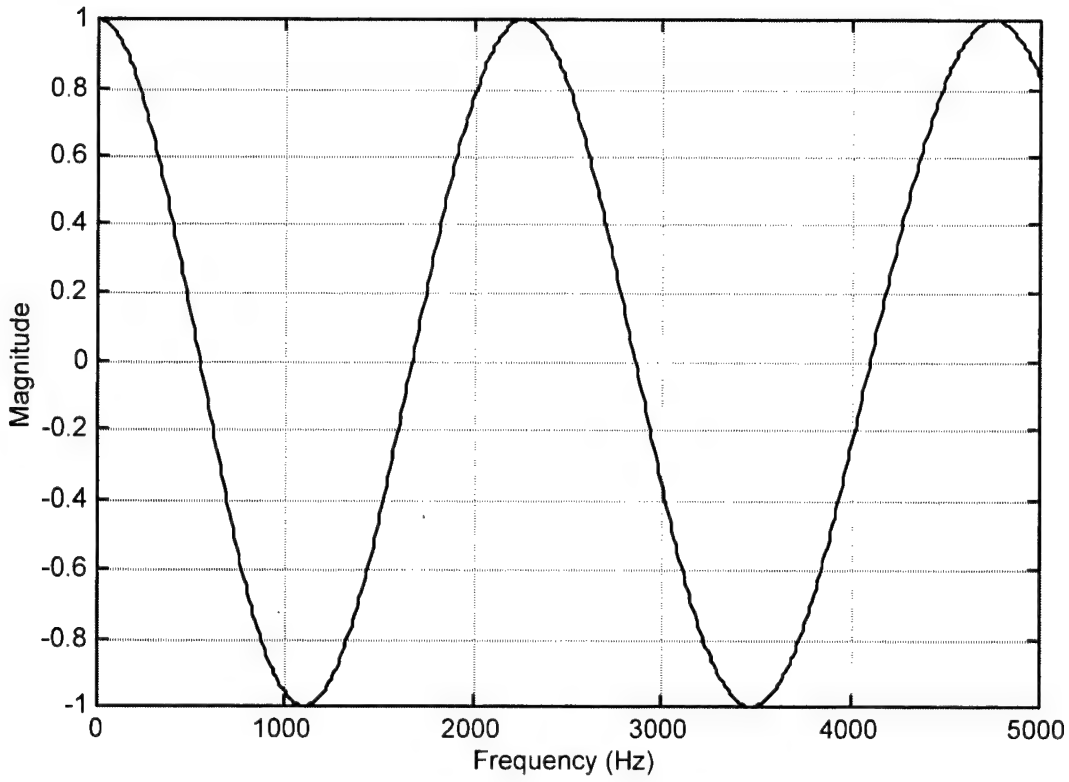

Figure 6. Function s Versus Frequency

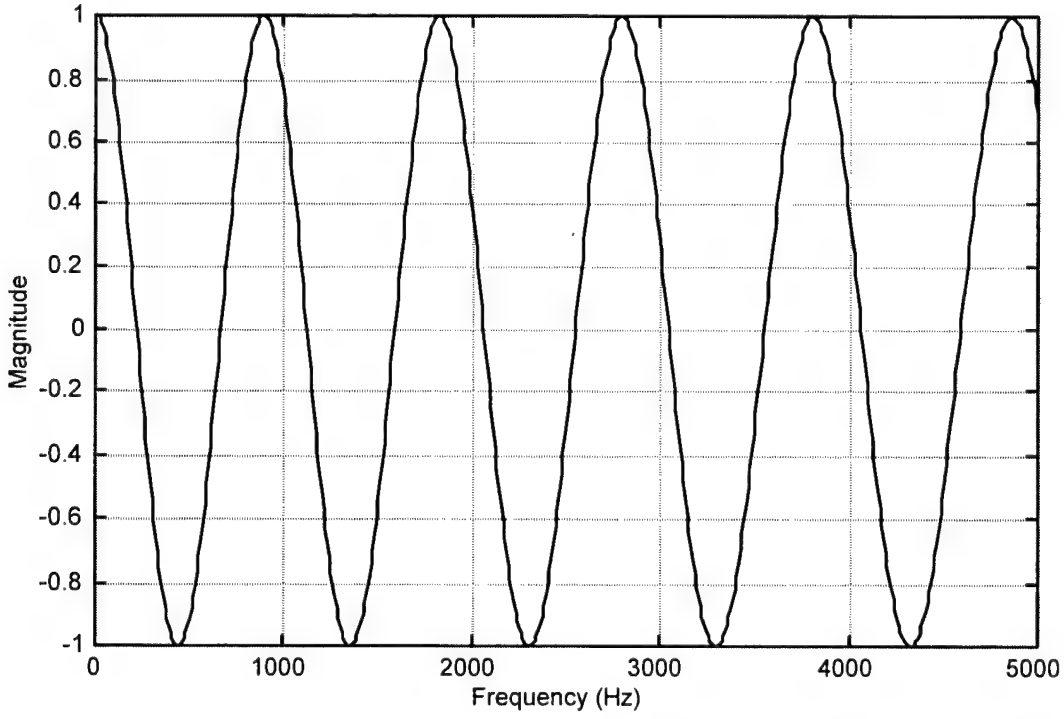

Figure 7. Function r Versus Frequency

Figure 8 shows actual and estimated dilatational wavespeed versus frequency for a system without mass for no additive noise, 2% additive noise, and 4% additive noise. This plot corresponds to the solution determined from equations (93)–(95). Figure 9 shows actual and estimated shear wavespeed versus frequency without mass for no additive noise, 2% additive noise, and 4% additive noise. This plot corresponds to the solution determined from equations (96)–(98).

Figure 10 plots actual and estimated shear modulus versus frequency for a system without mass for no additive noise, 2% additive noise, and 4% additive noise and is constructed using equation (103). Figure 11 shows actual and estimated Young's modulus versus frequency for a system without mass for no additive noise, 2% additive noise, and 4% additive noise and is constructed using equations (103), (104), and (106).

Figure 12 illustrates actual and estimated real Poisson's ratio versus frequency for a system without mass for no additive noise, 2% additive noise, and 4% additive noise and was plotted using equation (105). Because the numerical example is formulated using a Poisson's ratio that is strictly real, no imaginary component is shown in this plot. Imaginary values of Poisson's ratio are possible, however, and have been shown to theoretically exist.[17]

Figure 13 is a plot of the transfer function of the system with mass for vertical motion versus frequency and corresponds to equation (59) with $M = 199\ \text{kg/m}^2$. Figure 14 is a plot of the transfer function of the system with mass for horizontal motion versus frequency and corresponds to equation (90) with $M = 199\ \text{kg/m}^2$. The plots in both figures are displayed without additive noise.

Figure 15 shows the magnitude of the surface given by equation (99) versus real and imaginary dilatational wavenumbers at 2000 Hz with an additive noise value of 0.04 for a system with mass. The actual value of the dilatational wavenumber is denoted with a square marker, and the estimated value (found using the identification of a local minimum) is shown on the plot with a circle marker. Figure 16 is a plot of the magnitude of the surface given by equation (100) versus real and imaginary shear wavenumbers at 2000 Hz with an additive noise value of 0.04 for a system with mass. The actual value of the shear wavenumber is denoted with a square marker, and the estimated value (found using the identification of a local minimum) is shown on the plot

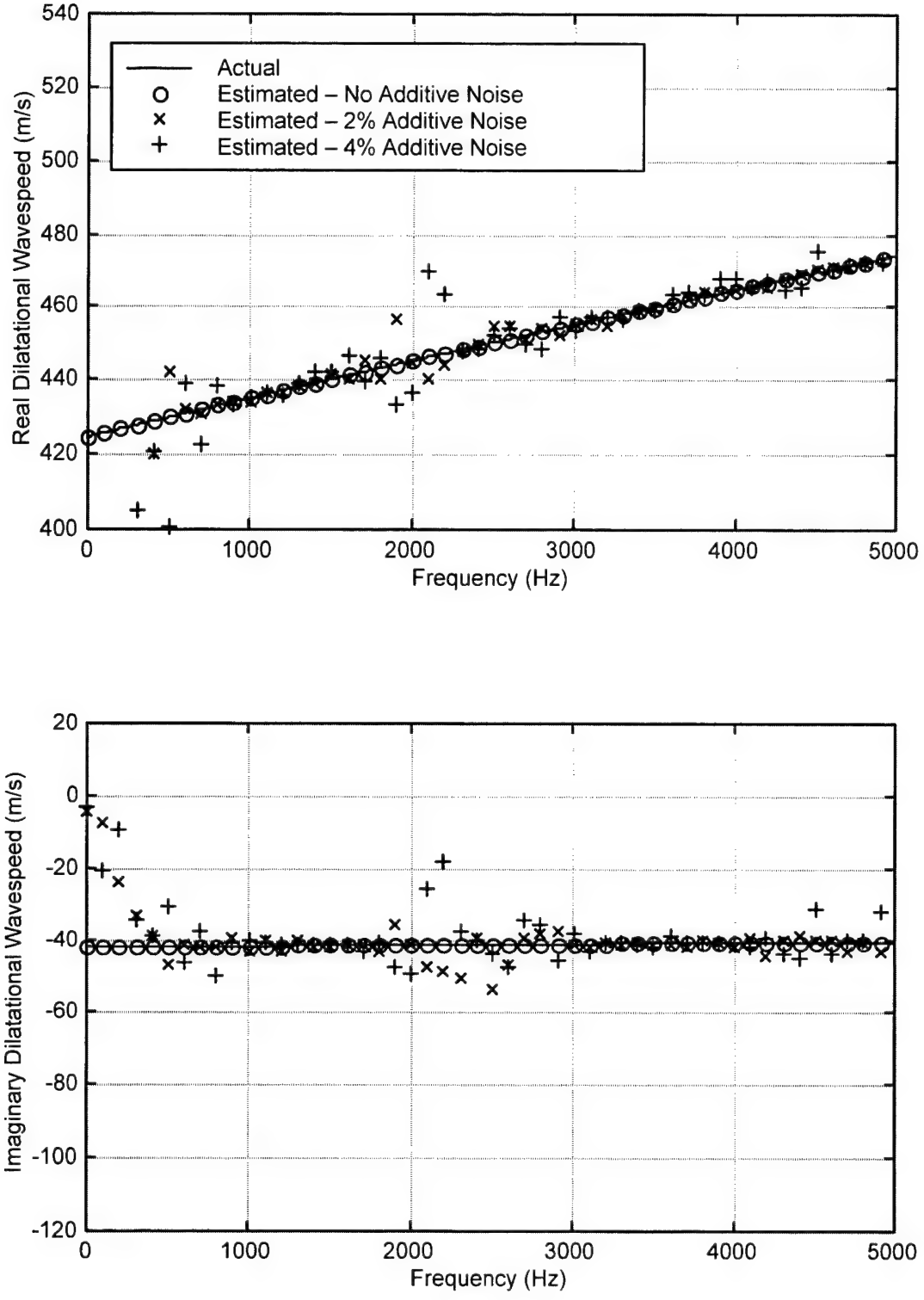

Figure 8. Actual and Estimated Dilatational Wavespeed Versus Frequency for System Without Mass

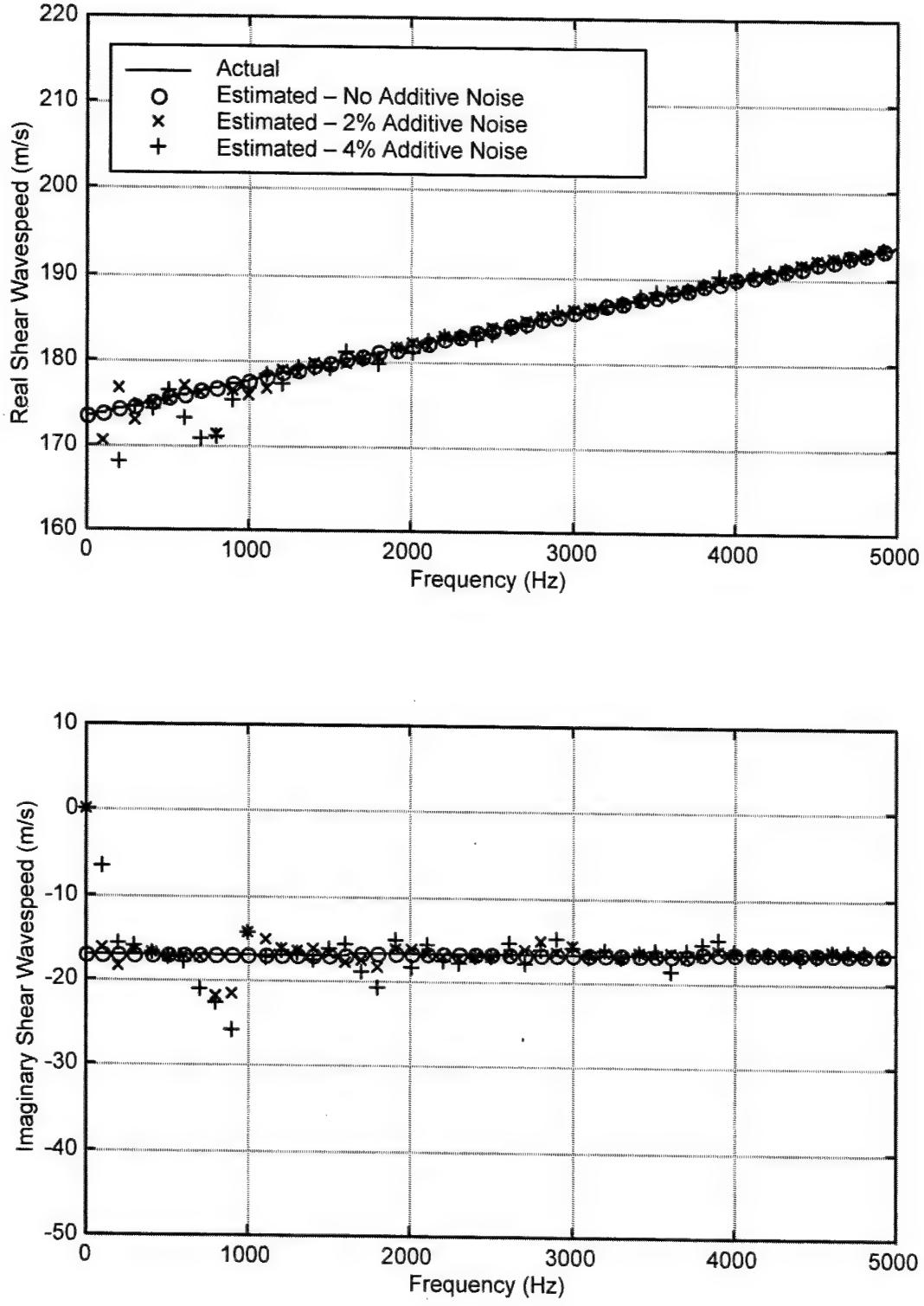

Figure 9. Actual and Estimated Shear Wavespeed Versus Frequency for System Without Mass

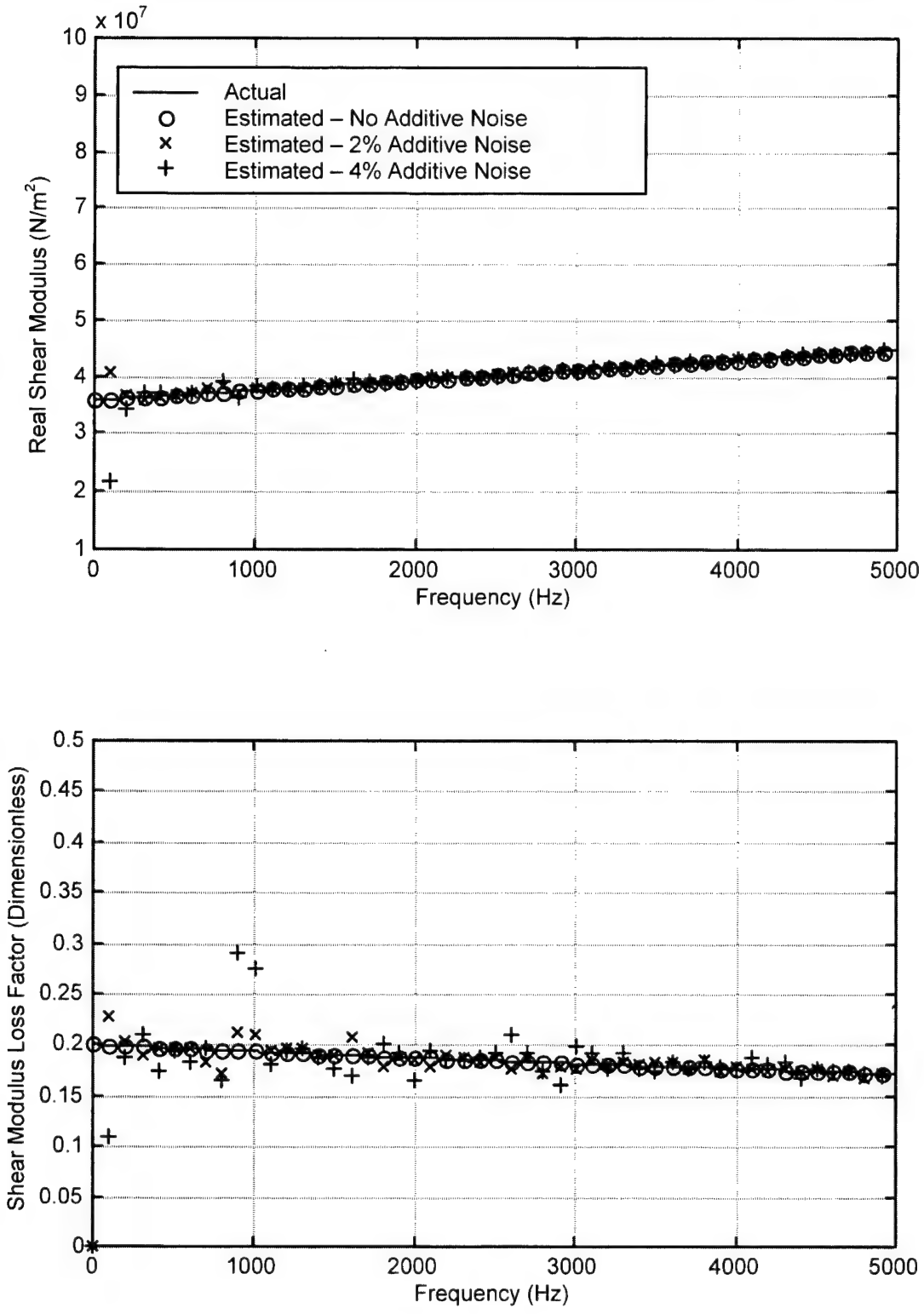

Figure 10. Actual and Estimated Shear Modulus Versus Frequency for System Without Mass

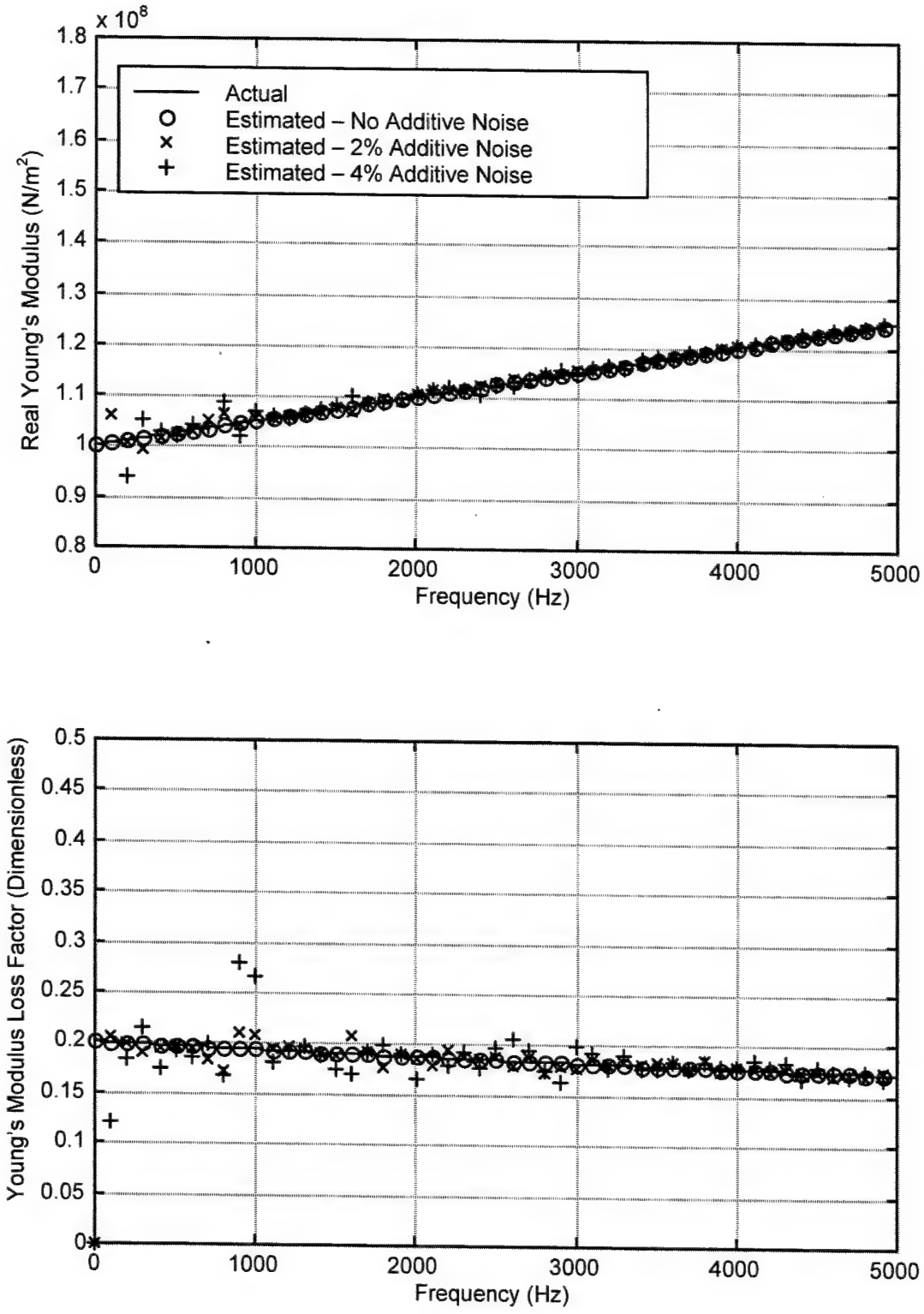

Figure 11. Actual and Estimated Young's Modulus Versus Frequency for System Without Mass

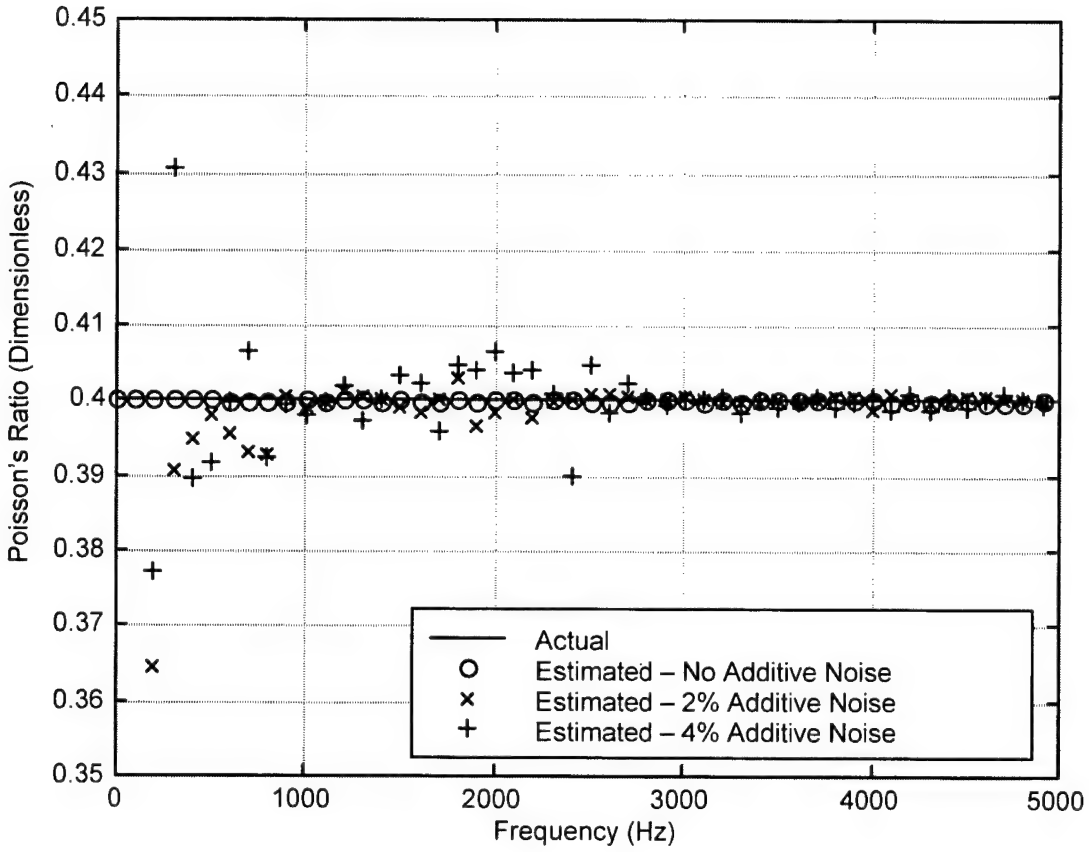

Figure 12. Actual and Estimated Real Poisson's Ratio Versus Frequency for System Without Mass

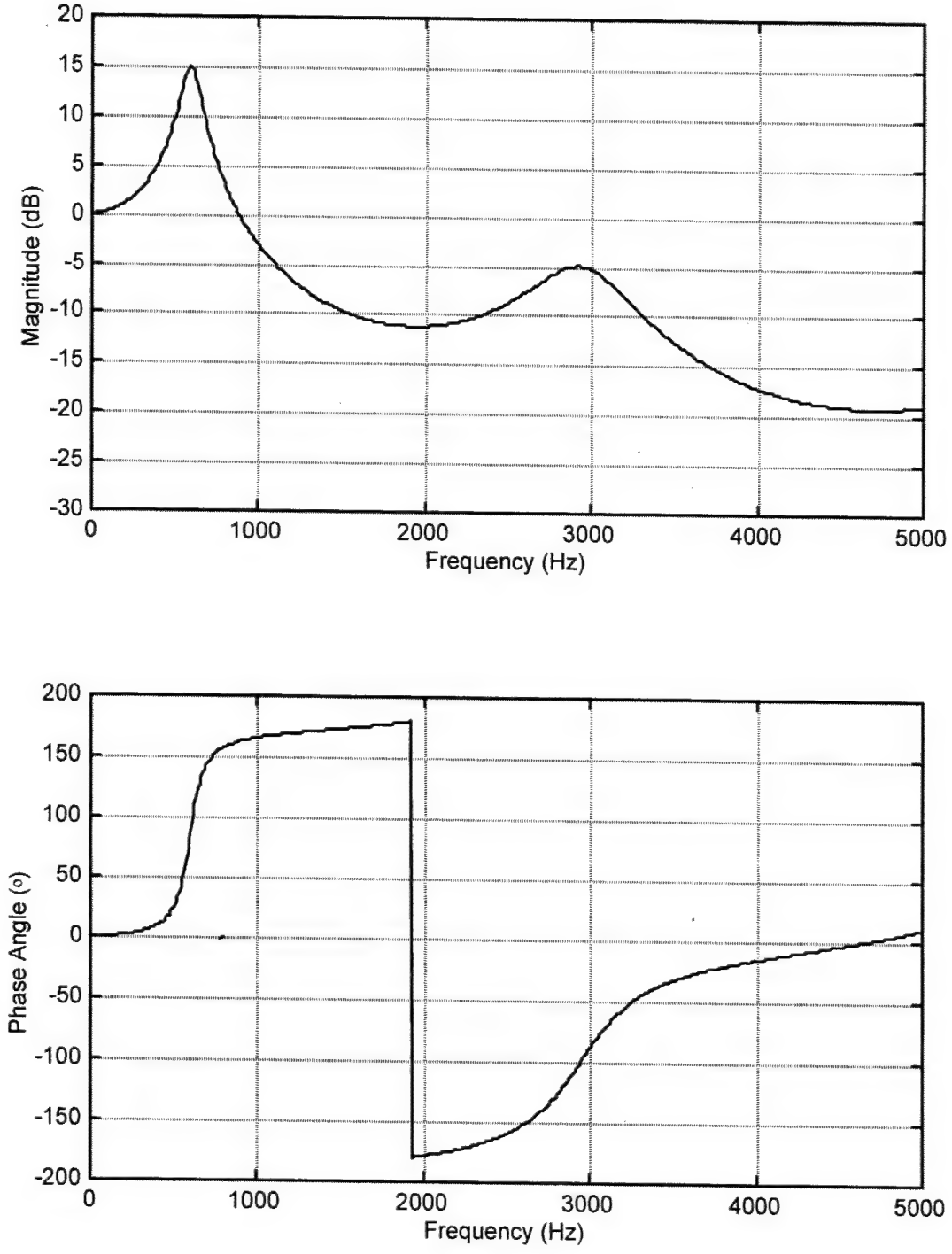

Figure 13. Transfer Function of Vertical Motion Versus Frequency for System With Mass

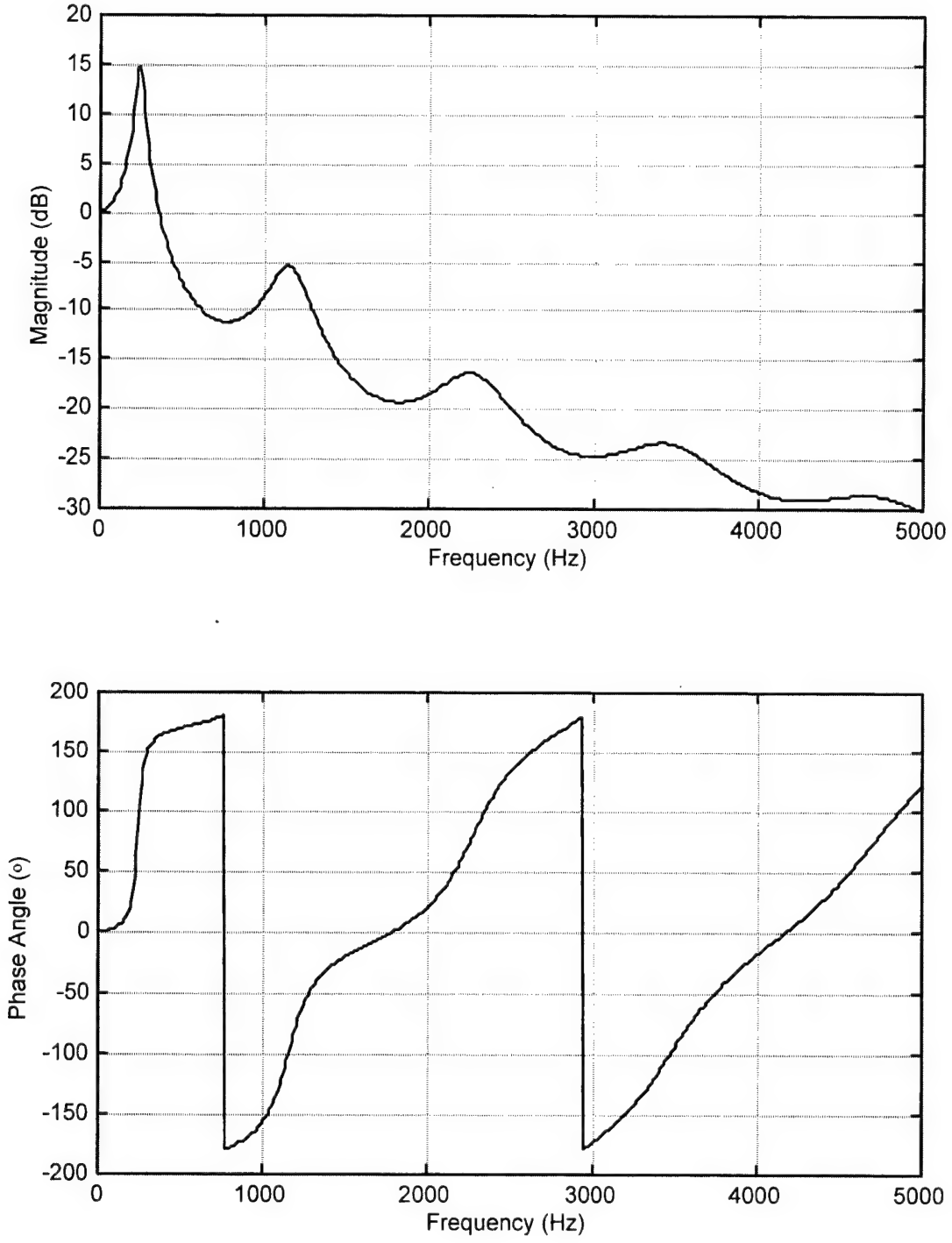

Figure 14. Transfer Function of Horizontal Motion Versus Frequency for System with Mass

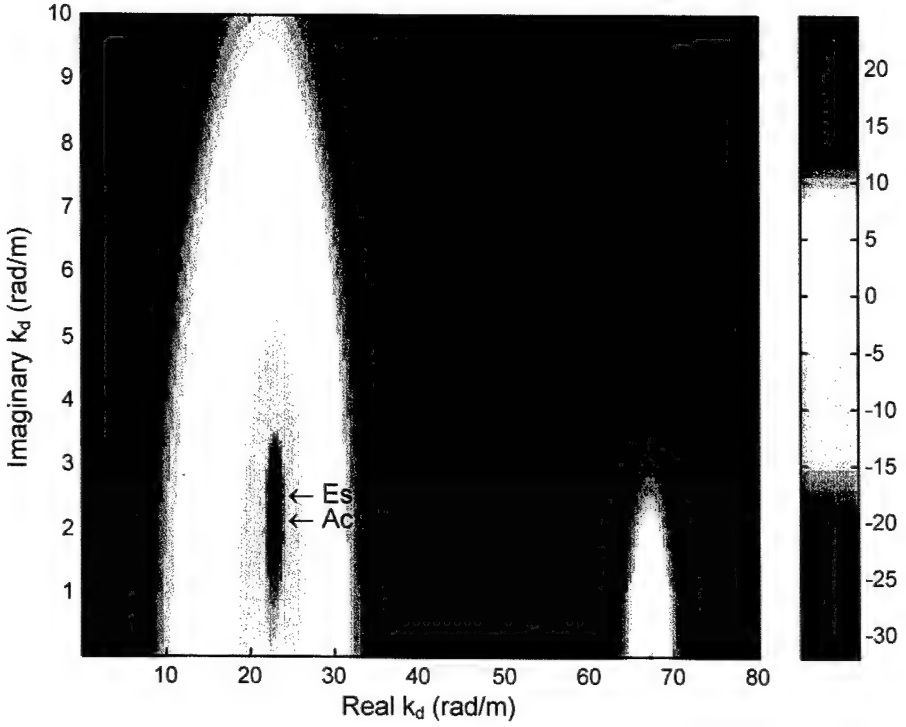

Figure 15. Magnitude of Surface Versus Real and Imaginary Dilatational Wavenumbers at 2000 Hz Showing Estimated and Actual Values for System with Mass and 0.04 Additive Noise

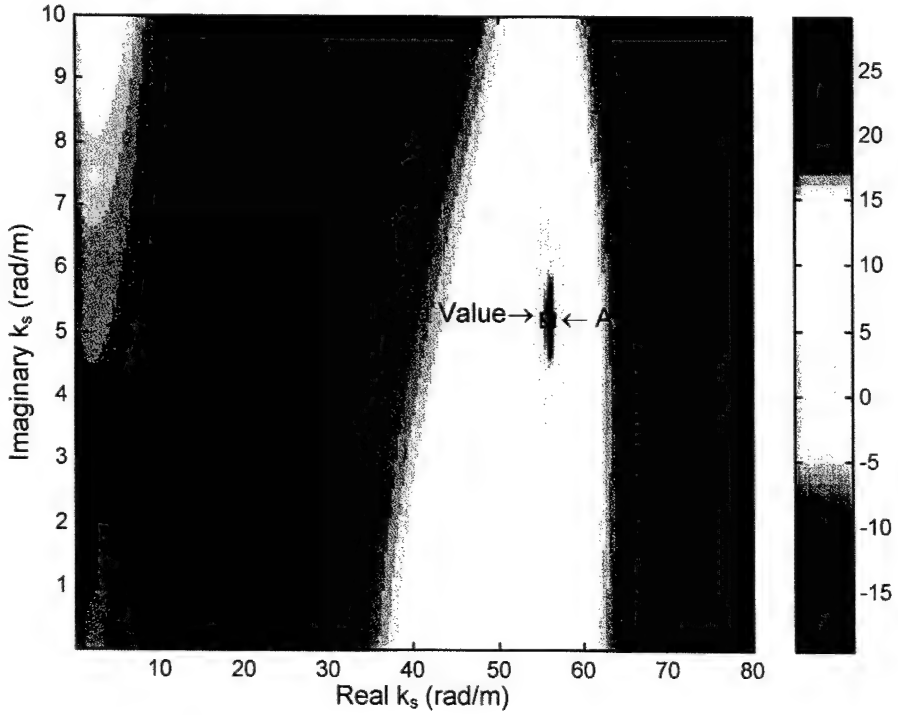

Figure 16. Magnitude of Surface Versus Real and Imaginary Shear Wavenumbers at 2000 Hz Showing Estimated and Actual Values for System with Mass and 0.04 Additive Noise

with a circle marker. These figures were constructed using 200 discrete points in both axis directions. The identification process was repeated every 100 Hz with a frequency spectrum of 50 to 5000 Hz.

Figure 17 is a plot of actual and estimated dilatational wavespeed versus frequency for a system with mass for no additive noise, 2% additive noise, and 4% additive noise. Figure 18 shows the actual and estimated shear wavespeed versus frequency for a system with mass for no additive noise, 2% additive noise, and 4% additive noise. Figure 19 plots actual and estimated shear modulus versus frequency for a system with mass for no additive noise, 2% additive noise, and 4% additive noise. The step-shaped results in the real part of figures 18 and 19 (upper plot) are due to the discretization size of the surfaces in equations (99) and (100). A discretization size finer than 200-by-200 points would produce less steplike (smoother) results. Figure 20 is a plot of actual and estimated Young's modulus versus frequency for a system with mass for no additive noise, 2% additive noise, and 4% additive noise. Figure 21 illustrates actual and estimated real Poisson's ratio versus frequency for a system with mass for no additive noise, 2% additive noise, and 4% additive noise.

Table 1 presents additive noise versus parameter estimation error for the system without mass and table 2 for the system with mass. The parameter estimation error was determined from the equation

$$\theta = \frac{1}{N}\sum_{n=1}^{N}\frac{\left|\kappa_{est}(\omega_n) - \kappa_{act}(\omega_n)\right|}{\left|\kappa_{act}(\omega_n)\right|}, \tag{109}$$

where θ is the parameter estimation error, $\kappa_{est}(\omega_n)$ is the estimated value of the parameter at the nth frequency value, $\kappa_{act}(\omega_n)$ is the actual value of the parameter at the nth frequency value, and N is the total number of frequencies at which an estimate is computed. Because the routine did not produce a realistic estimate of the parameters at very low frequencies, these parameters are not included in the tables. All the parameters are estimated with very small error. Based on the results shown in each table, it is found that the grid method produces a more accurate estimate of the parameters than does the numerical solution method for data with noise.

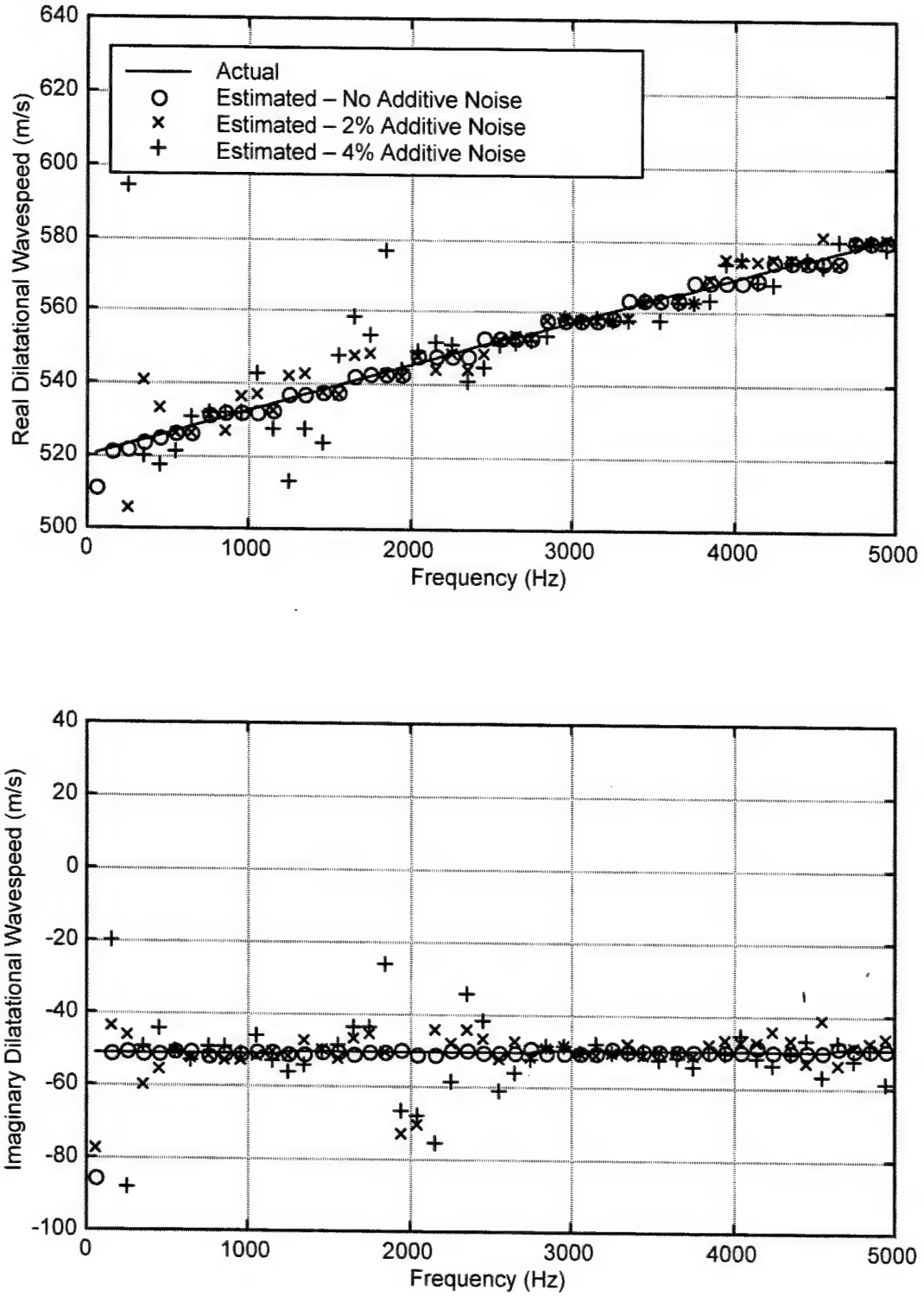

Figure 17. Actual and Estimated Dilatational Wavespeed Versus Frequency for System with Mass

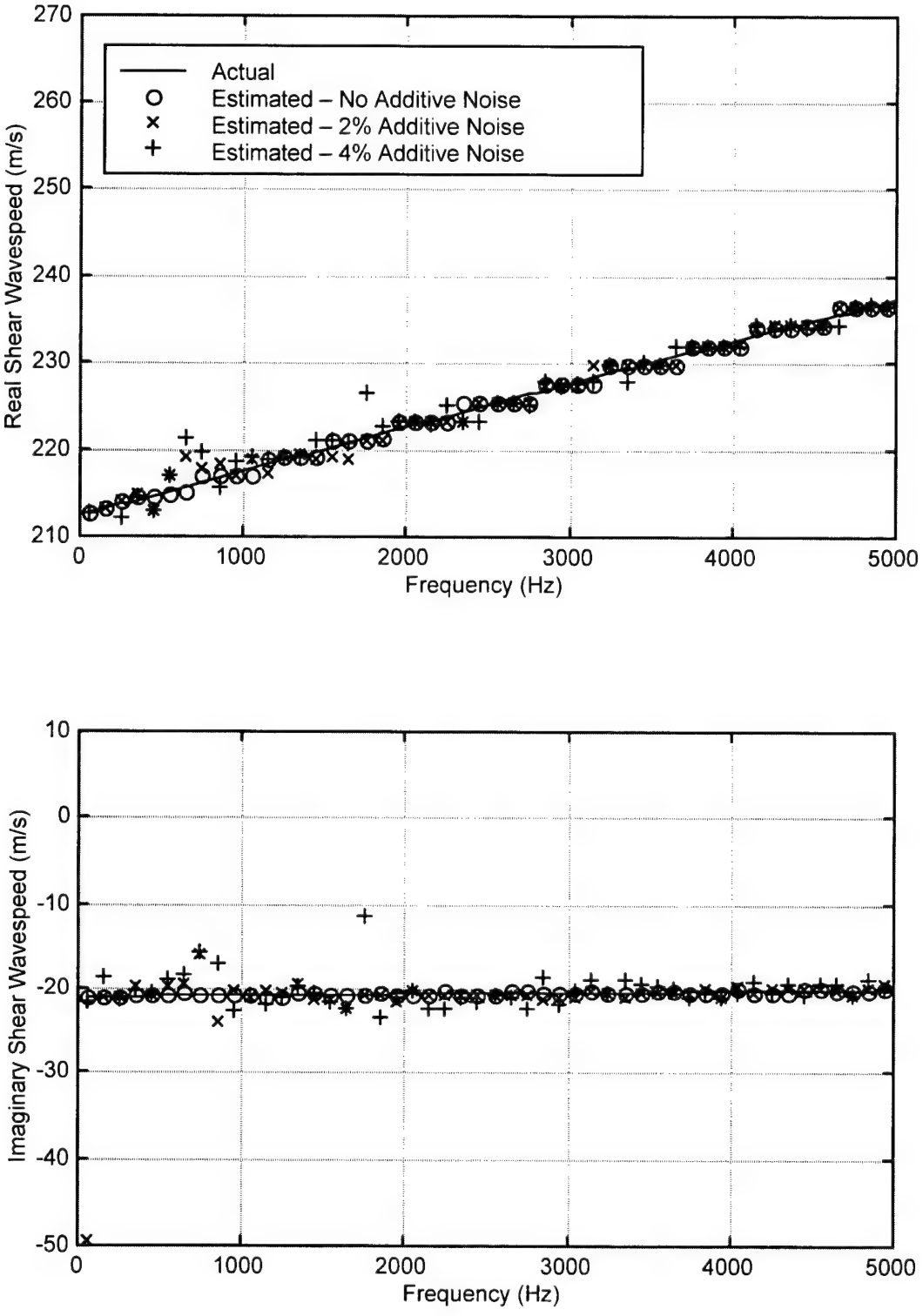

Figure 18. Actual and Estimated Shear Wavespeed Versus Frequency for System with Mass

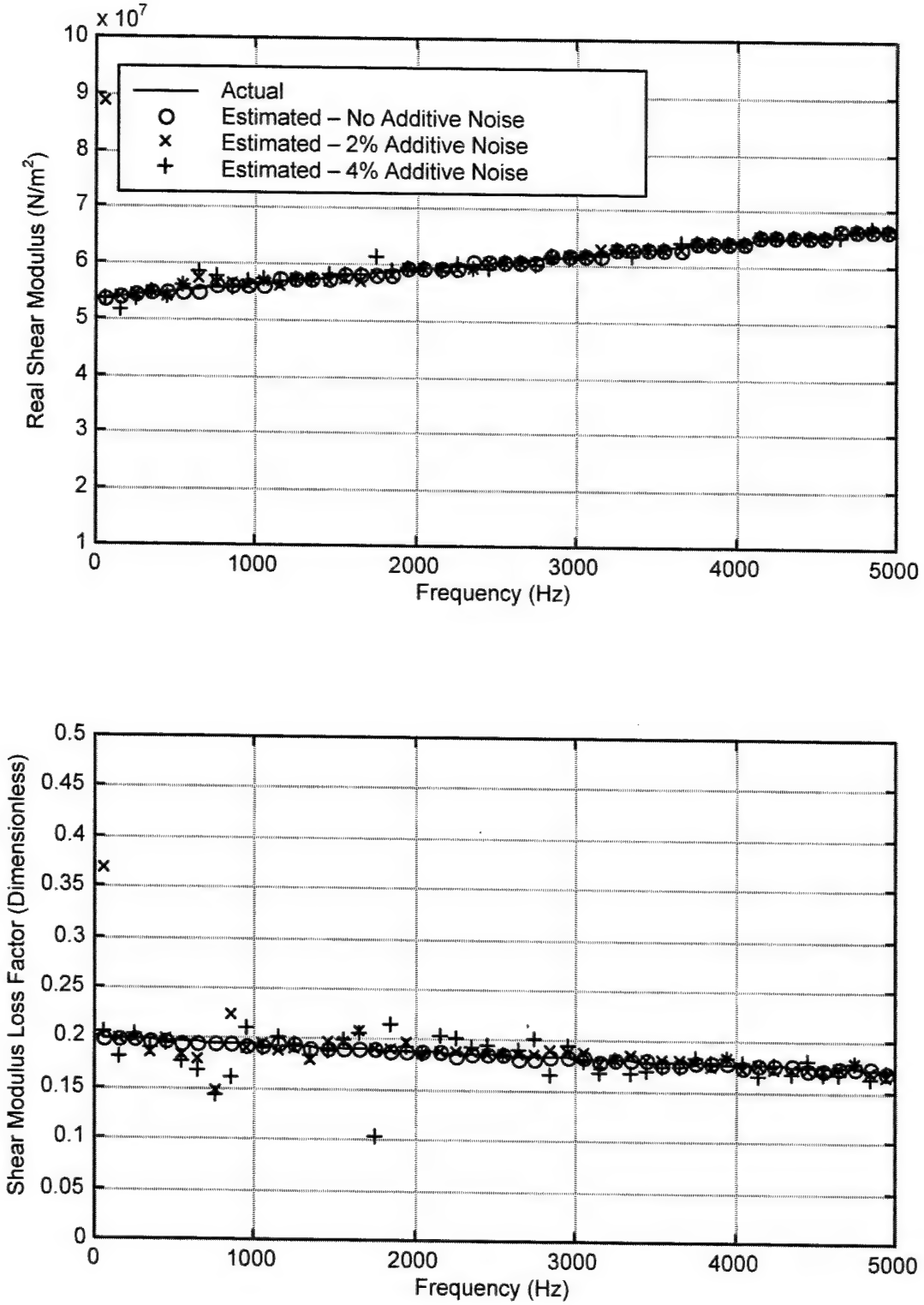

Figure 19. Actual and Estimated Shear Modulus Versus Frequency for System with Mass

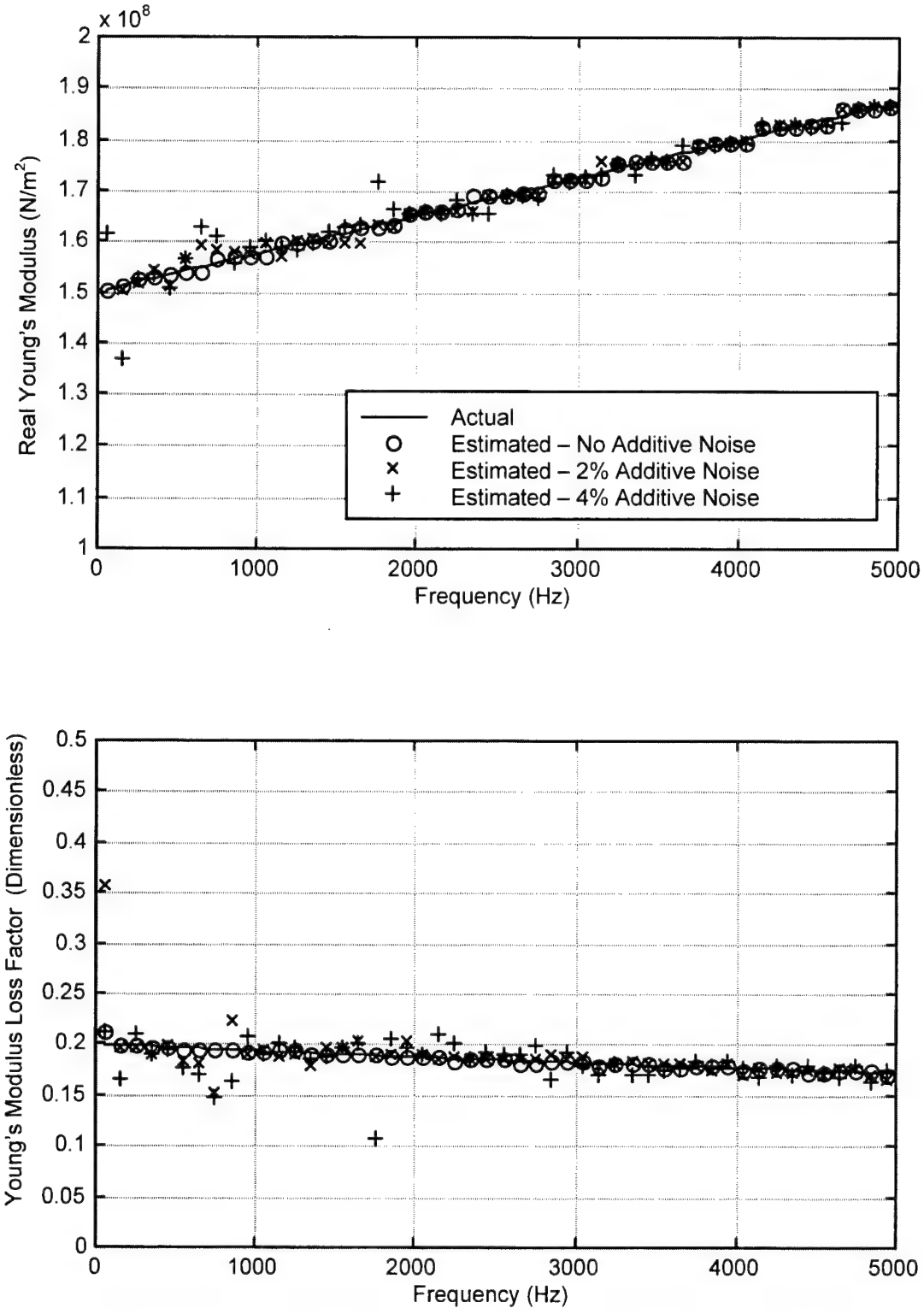

Figure 20. Actual and Estimated Young's Modulus Versus Frequency for System with Mass

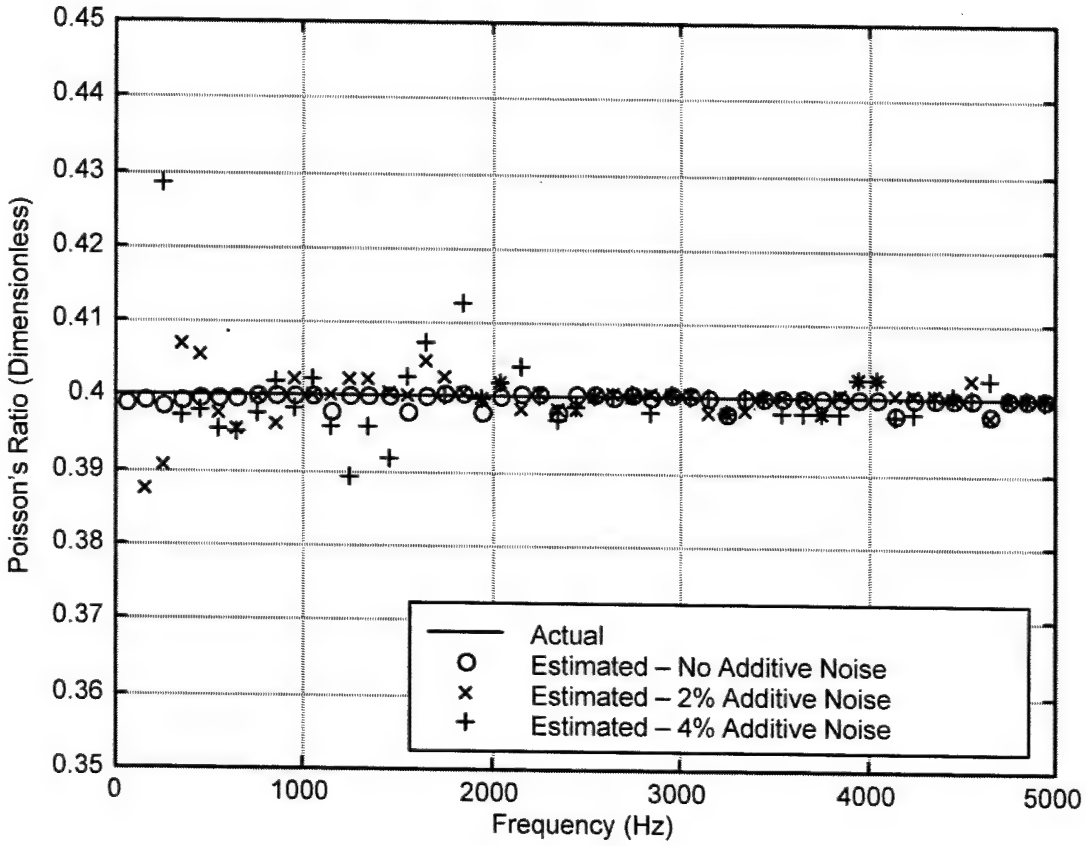

Figure 21. Actual and Estimated Real Poisson's Ratio Versus Frequency for System with Mass

Table 1. Additive Noise Versus Parameter Estimation Error for System Without Mass

Parameter	Additive Noise	Parameter Estimation Error
c_d	0	~0
c_d	0.020	0.021
c_d	0.040	0.027
c_s	0	~0
c_s	0.020	0.0051
c_s	0.040	0.0099
G	0	~0
G	0.020	0.012
G	0.040	0.020
E	0	~0
E	0.020	0.015
E	0.040	0.022
υ	0	~0
υ	0.020	0.013
υ	0.040	0.017

Table 2. Additive Noise Versus Parameter Estimation Error for System with Mass

Parameter	Additive Noise	Parameter Estimation Error
c_d	0	0.0023
c_d	0.020	0.0076
c_d	0.040	0.013
c_s	0	0.0024
c_s	0.020	0.0046
c_s	0.040	0.0071
G	0	0.0047
G	0.020	0.0092
G	0.040	0.014
E	0	0.0045
E	0.020	0.0087
E	0.040	0.013
υ	0	0.0012
υ	0.020	0.0030
υ	0.040	0.0051

9. CONCLUSIONS AND RECOMMENDATIONS

This report documents the derivation of a theoretical method for estimating the mechanical properties of slab-shaped materials subjected to compressional forces. After a single thick plate is vibrated both vertically and horizontally and the transfer functions between the faces of the plate are measured, estimations of dilatational wavespeed, shear wavespeed, Young's modulus, shear modulus, and Poisson's ratio can be accurately obtained. Further investigation showed that this technique is relatively immune to noise mechanisms that are sometimes present in the measurements.

It is recommended that actual measured data be used in a laboratory setting to evaluate the effectiveness of the inverse method.

10. REFERENCES

1. D. M. Norris Jr., and W. C. Young, "Complex Modulus Measurements by Longitudinal Vibration Testing," *Experimental Mechanics*, vol. 10, 1970, pp. 93-96.

2. W. M. Madigosky and G. F. Lee, "Improved Resonance Technique for Materials Characterization," *Journal of the Acoustical Society of America*, vol. 73, no. 4, 1983, pp. 1374-1377.

3. S. O. Oyadiji and G. R. Tomlinson, "Determination of the Complex Moduli of Viscoelastic Structural Elements by Resonance and Non-Resonance Methods," *Journal of Sound and Vibration*, vol. 101, no. 3, 1985, pp. 277-298.

4. S. L. Garrett, "Resonant Acoustic Determination of Elastic Moduli," *Journal of the Acoustical Society of America*, vol. 88, no. 1, 1990, pp. 210-220.

5. J. L. Buchanan, "Numerical Solution for the Dynamic Moduli of a Viscoelastic Bar," *Journal of the Acoustical Society of America*, vol. 81, no. 6, 1987, pp. 1775-1786.

6. T.-K. Ahn and K.-J. Kim, "Sensitivity Analysis for Estimation of Complex Modulus of Viscoelastic Materials by Non-Resonance Method," *Journal of Sound and Vibration*, vol. 176, no. 4, 1994, pp. 543-561.

7. A. J. Hull, "An Inverse Method to Measure the Axial Modulus of Composite Materials Under Tension," *Journal of Sound and Vibration*, vol. 195, no. 4, 1996, pp. 545-551.

8. S. I. Roklin and W. Wang, "Measurements of Elastic Constants of Very Thin Anisotropic Plates," *Journal of the Acoustical Society of America*, vol. 94, no. 5, 1993, pp. 2721-2730.

9. V. Marchand, J. Authesserre, J. Pouyet, and C. Bacon, "Determination of the Elastic Constants of Materials, in the Form of Plates, by a Free Vibration Method," *Journal of Sound and Vibration*, vol. 194, no. 4, 1996, pp. 497-512.

10. F. Moussu and M. Nivoit, "Determination of Elastic Constants of Orthotropic Plates by a Modal Analysis/Method of Superposition," *Journal of Sound and Vibration*, vol. 165, no. 1, 1993, pp. 149-163.

11. A. J. Hull, "A Method for Estimating the Mechanical Properties of a Solid Material Subjected to Insonification – Part I: Theory," NUWC-NPT Technical Report 11,404, Naval Undersea Warfare Center Division, Newport, RI, 6 December 2002.

12. J. E. Cole III and K. Martini, "Low-Frequency Impedance Measuring Device for Underwater Acoustic Material," *Journal of the Acoustical Society of America*, vol. 95, no. 5, part 2, 1994, p. 2931.

13. S. Beretti, C. Audoly, and P. Guillaussier, "Pressure Effects on the Dynamic and Static Properties of Perforated Elastomers Used in Underwater Acoustics," *Journal of the Acoustical Society of America*, vol. 97, no. 5, part 2, 1995, p. 3293.

14. V. E. Glazanov and A. V. Mikhailov, "Calculation of the Velocity of Sound in Rubber Containing Cylindrical Voids with Allowance for Dynamic Correction," *Acoustical Physics*, vol. 47, no. 6, 2001, pp. 671-676.

15. J. D. Dickens, "Phase Velocity of Rubber Element in Vibration Isolator Under Static Load," *Journal of Sound and Vibration*, vol. 234, no. 1, 2000, pp. 21-42.

16. J. D. Dickens, "Dynamic Model of Vibration Isolator Under Static Load," *Journal of Sound and Vibration*, vol. 236, no. 2, 2000, pp. 323-337.

17. T. Pritz, "Frequency Dependencies of Complex Moduli and Complex Poisson's Ratio or Real Solid Materials," *Journal of Sound and Vibration*, vol. 214, no. 1, 1998, pp. 83-104.

INITIAL DISTRIBUTION LIST

Addressee	No. of Copies
Office of Naval Intelligence (ONI 241 – J. Zilius, T. Morgan; ONI 263 – S. Brown (2))	4
Office of Naval Research (ONR 321 – R. Elswick; ONR 333 – K. Ng)	2
Defense Technical Information Center	2
Center for Naval Analyses	1